JOURNAL OF GEOPHYSICAL RESEARCH, VOL. 101, NO. C9, PAGES 20,833–20,848, SEPTEMBER 15, 1996

A simple model study of the Arctic Ocean freshwater balance, 1979–1985

Michael Steele, Don Thomas, and Drew Rothrock

Polar Science Center, Applied Physics Laboratory, College of Ocean and Fishery Sciences, University of Washington, Seattle

Seelye Martin

Department of Oceanography, College of Ocean and Fishery Sciences, University of Washington, Seattle

Abstract. The freshwater budget of the Arctic Ocean from autumn 1979 to autumn 1985 is examined using a simple ice-ocean model. The ice model, described in detail by *Thomas et al.* [this issue], uses data from drifting buoys to determine the velocity field and data from passive microwave satellites to determine the concentration field. The resulting fluxes of momentum and salt are then used to drive the ocean model. The model "grid" consists of seven broad regional cells in which we compute average quantities such as salinity profiles. The domain extends down to 200 m depth. The results indicate that the interannual variability of mixed layer salinity (MLS) is greater in the western Arctic than in the eastern Arctic. The interannual variability of MLS in the Arctic Ocean as a whole is quite small in this simulation but is still as large or larger than the trend predicted by *Manabe et al.* [1991] due to increasing atmospheric CO_2. The results of our freshwater analysis indicate that there was an increase of 45% above the mean in the freshwater export through Fram Strait during 1982. This increase occurred in both the sea ice and ocean components, although mostly in the former. A decrease in the freshwater outflow through the Canadian Archipelago (which generally constitutes about 34% of the total) occurred at about the same time. Finally, a simple experiment was run in which river and precipitation fluxes were increased to the level predicted by *Manabe et al.* [1991] by the end of a 100-year increased CO_2 simulation. The resulting increase in oceanic freshwater flux through the Canadian Archipelago is about 60% more than that through the Fram Strait, which might have an influence on the preferred location for deep water formation in a warmer climate.

1. Introduction

Evaporation over the North Atlantic Ocean is about twice that over the North Pacific Ocean, while precipitation rates are about equal [*The Open University*, 1989, p. 200]. The result is that the average salinity of the Atlantic Ocean is higher (34.9 ppt) than that of the Pacific Ocean (34.6 ppt). The situation would be more extreme except for the presence of a "back door," the Arctic Ocean, through which this freshwater imbalance can partially equilibrate. Also, about 10% of the world's river runoff enters the Arctic Ocean, flowing into a basin that occupies only 6% of the global ocean surface area. Thus the Arctic is a great estuary, transferring freshwater from rivers and the North Pacific into the northeast Atlantic via Fram Strait and into the northwest Atlantic via the complex channels of the Canadian Archipelago.

Associated with the imbalance in freshwater between the North Pacific and the North Atlantic Oceans is a difference in the average stratification, which allows deep waters to form (via convection) in the Atlantic but not in the Pacific. In the limit of an infinitely fast transfer rate of freshwater through the Arctic, this imbalance would be removed and convection in the North Atlantic might cease. However, *Aagaard and Carmack* [1989] and *Häkkinen* [1993] have shown that this scenario is unnecessarily extreme: in fact, small and subtle changes in the freshwater outflow via Fram Strait may be sufficient to substantially influence deep water formation in the Greenland Sea. Unfortunately, the interannual variability of this flow is uncertain, and the overall freshwater budget of the Arctic Ocean is poorly understood. Some of the key components of this budget are well-constrained by observations, such as the flow through Bering Strait, while others are less so, such as the flow through the Canadian Archipelago.

Observations suggest the existence of significant interannual variability in the formation of deep water both in the northeast Atlantic [*Dickson et al.*, 1988] and in the northwest Atlantic [*Talley and McCartney*, 1982; *Clarke and Gascard*, 1983]. Recent chemical tracer analyses by *Schlosser et al.* [1991] indicate that there was a decrease in the rate of deep water formation in the Greenland Sea during the early 1980s. This is the period of satellite observations of sea ice coverage by the Scanning Multichannel Microwave Radiometer (SMMR) [*Cavalieri et al.*, 1984] and of sea ice motion by the Arctic Buoy Program [*Untersteiner and Thorndike*, 1982]. The assimilation of these data into a sea ice model has been discussed in a companion paper [*Thomas et al.*, this issue, hereinafter TRMS]. Here we discuss the coupling of the ice model to a simple ocean model in order to examine the freshwater balance of the Arctic Ocean.

In the following section, the ice and ocean models are described, including the satellite and other data that are used for forcing, initialization, and boundary conditions. In section 3, the

Paper number 96JC01686.
0148-0227/96/96JC-01686$09.00

results of the model are presented in terms of mixed layer salinities and volume transports. In section 4, we present the corresponding freshwater transports and budgets; both the annual average and seasonal/interannual variability are discussed. Also, the response of the model to an increase in freshwater inputs such as observed in the climate simulation of *Manabe et al.* [1991] is presented. Conclusions are presented in section 5.

2. The Model

The domain of our simulation consists of a simple grid of seven "cells," or regions, shown in Figure 1. The surface areas of the cells are given in Table 1, while information about the boundaries between cells is presented in Table 2. The cells were chosen mostly for the convenience of SMMR sea ice data assimilation, and capture the gross circulation features such as the Beaufort Gyre and the Transpolar Drift Stream (TRMS). Note that the domain excludes the Barents and Kara seas. The western Arctic is here defined as the Beaufort Sea, Chukchi Sea, Central Arctic, and Canada Basin cells; the eastern Arctic is defined as the Laptev Sea, North Pole, and Nansen Basin cells. The model covers the upper 200 m of the ocean, which contains the surface and halocline waters where the bulk of the freshwater in the Arctic Ocean lies. (The bottom depth of 200 m was chosen to represent an Arctic-average halocline base depth. It is also roughly the maximum depth of the freshwater-containing "Polar Water" in the East Greenland Current, as defined by *Aagaard and Coachman* [1968].) The salinity at 200 m depth is generally less than or equal to the freshwater reference salinity (section 4), so that upwelling and downwelling of freshwater at this depth is allowed.

The model is an extension of the traditional one-dimensional Arctic model such as described, for example, by *Björk* [1989]. Inflows and outflows at the perimeter of our domain are parameterized as in *Björk* [1989] and are described in more detail below.

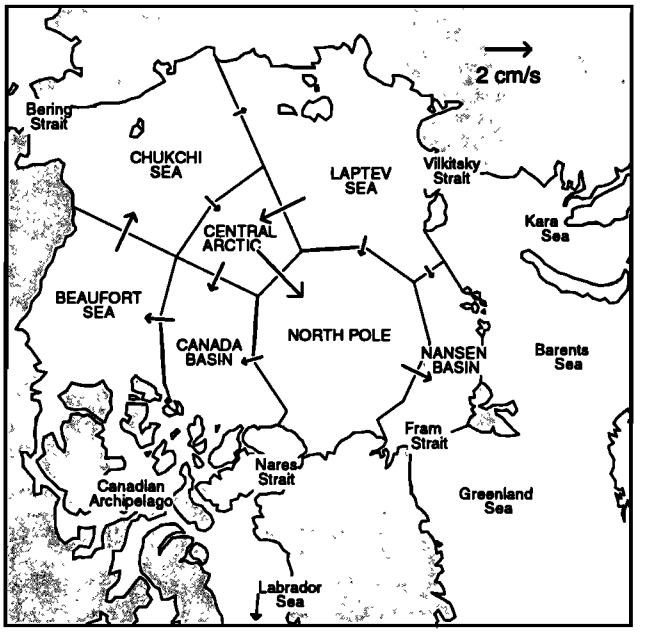

Figure 1. The model grid, consisting of seven "cells." The western Arctic consists of the Beaufort Sea, Chukchi Sea, Central Arctic, and Canada Basin cells. The eastern Arctic consists of the Laptev Sea, North Pole, and Nansen Basin cells. The surface geostrophic velocity field derived from the Levitus data is also shown.

Table 1. Cell Areas, in 10^6 km^2

Cell	Area
Beaufort Sea	0.96
Chukchi Sea	1.33
Canada Basin	0.70
Central Arctic	0.44
Laptev Sea	1.57
North Pole	1.41
Nansen Basin	0.52
Total	6.92

The main innovation is simply the coupling of a small number of these models together to provide a rough picture of geographic variation and to examine individual inflow/outflow locations at the perimeter of the Arctic Ocean. The coupling between cells is also discussed below; it is parameterized in a manner similar to that of *Piacsek et al.* [1991]. We argue below that the main results of our simulation are qualitatively insensitive to the parameterization of intercell transports.

For comparison, an additional simulation is also performed, in which the entire domain is one large cell. This is the traditional "one-dimensional" simulation, assuming horizontal homogeneity across the entire basin. The results are then compared to an Arctic Ocean average formed by area-weighted averaging of the individual cell results.

The coupling between the sea ice and ocean models is one-way. The ocean model uses, as surface boundary conditions, the (1) ice-ocean stress and (2) salt fluxes from ice melt minus growth. The latter assumes a constant surface salinity of 31.5 ppt. This value would vary in a fully coupled model, changing the predicted fluxes by less than 10% for typical surface salinity variations. The surface fluxes from the ice model are truncated to produce a 6-year time series from autumn 1979 to autumn 1985. This introduces small differences between annual mean ice-ocean surface fluxes in TRMS and in this study. Other effects not included in our model are (1) the influence of ocean currents on the sea ice motion, which are not needed here since we use observed buoy motions and a free drift model, and (2) oceanic heat flux which might be used to melt ice, which is unnecessary owing to our use of a fixed ice thermodynamic seasonal cycle and ice concentration observations.

2.1. Ice Model

The ice model is described in detail in TRMS, and is only summarized here. Ice thickness distributions are computed for each of the seven cells shown in Figure 1. The ice model consists of ridging and thermodynamics (both described by *Thorndike et al.* [1975]), and advection (based on buoy motions and winds). The thermodynamic model consists of a climatological look-up table that is a function of both thickness and time of year, but does not vary regionally. This simplification of ice thermodynamics creates unrealistically low summer melting in the more southerly cells. To compensate for this, TRMS adjust the model estimates of ice concentration to fit those derived by Kalman smoothing of SMMR

Table 2. Cell Boundary Information

Boundary	Length, km	Type	Level of No Motion, m
Beaufort Sea - Chukchi Sea	817	interior	200
Beaufort Sea - Canada Basin	1022	"	"
Central Arctic - Canada Basin	654	"	"
Chukchi Sea - Central Arctic	906	"	"
Chukchi Sea - Laptev Sea	828	"	"
Canada Basin - North Pole	999	"	"
Central Arctic - North Pole	445	"	"
Central Arctic - Laptev Sea	654	"	"
Laptev Sea - North Pole	890	"	"
Laptev Sea - Nansen Basin	262	"	"
North Pole - Nansen Basin	1257	"	"
Nansen Basin - Greenland Sea	230	outflow	"
North Pole - Canadian Arch.	50	outflow	"
Beaufort Sea - Canadian Arch.	125	outflow	150
Canada Basin - Canadian Arch.	100	outflow	150
Bering Sea - Chukchi Sea	75	inflow	---
Kara Sea - Laptev Sea	150	inflow	---

The latitude and longitude of each cell node is given in Appendix B of *Thomas and Rothrock* [1993].

observations. Also included in the model of TRMS is a parameterization for ice-ocean salt fluxes that result from ice growth, melt, and brine drainage. These are then converted to salinity fluxes for use in the ocean model (section 2.2) and are presented in Figure 3 below as freshwater fluxes. (The definition of freshwater is given in section 4.) While the use of climatological ice thermodynamics may somewhat reduce the spatial and temporal variability in the resulting freshwater fluxes, TRMS argue that the assimilation of observed concentration data preserves much of the real variability.

2.2. Ocean Model

We focus here on the freshwater balance of the Arctic Ocean. The heat balance is not considered, since the sea ice model uses climatological thermodynamics. Thus the ocean model consists only of equations for salinity and for velocity.

The average salinity S within each cell is determined by

$$\frac{\partial S}{\partial t} = -\frac{1}{A}\sum_{i=1}^{N} u_i S_i L_i - \frac{\partial (wS)}{\partial z} + \frac{\partial}{\partial z} K \frac{\partial S}{\partial z} \qquad (1)$$

The first term on the right-hand side of (1) is horizontal advection, where u_i is the velocity perpendicular to a boundary segment of length L_i (positive outward). On interior boundaries, the salinity S_i is calculated as the mean of the neighboring cells' salinities; on exterior boundaries it is the bounding cell's salinity S. Each cell of area A has a different number N of "active" boundary segments (those on which a velocity u_i is defined). The integrated flux divergence form is used here because the unusual grid makes the computation of horizontal gradients problematic.

The second term on the right-hand side of (1) is vertical advection, where the vertical velocity w is determined diagnostically by integrating the continuity equation from the top at $z = 0$,

$$w = -\int_0^z \left(\sum_{i=1}^{N} u_i L_i \right) dz \qquad (2)$$

and $w \equiv 0$ at the surface. The third term on the right-hand side of (1) is vertical diffusion. The turbulent diffusivity $K(z)$ is modeled here using the so-called "level 2.5" parameterization of *Mellor and Yamada* [1982] which contains prognostic equations for turbulent kinetic energy and turbulent length scale that are ultimately dependent on the mean shear and stratification. Another term that is often added to (1) is climate damping; we find it unnecessary in order to achieve equilibrium.

The horizontal velocity on each boundary is composed of two parts,

$$u_i = u_e + u_g \quad (3)$$

where u_e is the Ekman component and u_g is the geostrophic component. The Ekman velocity u_e across each boundary is forced by the daily ice motion fields discussed in section 2.1, using a logarithmic drag formula with a roughness z_o of 5 cm [*Mellor et al.*, 1986; *Mellor and Kantha*, 1989; *Riedlinger and Warn-Varnas*, 1990]. This velocity is applied on all intercell (or "interior") boundaries and on the exterior boundary at Fram Strait (Figure 1).

On the internal boundaries, the geostrophic velocity u_g is computed a priori from the Levitus data set [*Levitus*, 1982] using the thermal wind relationship and thereafter is fixed for all time, following *Piacsek et al.* [1991]. To do this, we computed a three-dimensional field of u_g from the annual mean Levitus data on a 40-km grid and averaged the resulting vectors to obtain transports across our cell boundaries. These velocities are computed relative to 200 m depth and are thus relative to the flow of salty Atlantic Water that lies between 200 and 600 m depth. They are then interpolated from the Levitus depth levels to the vertical spacing of our model (described below in section 2.5). Our 40 km surface velocity field looks very similar to that produced by *Piacsek et al.* [1991] and shown in their Figure 11b.

Calculated surface values of u_g are shown in Figure 1. The field is qualitatively similar to the average ice motion (TRMS) in the Beaufort Gyre. Like the ice motion field, there is a strong transport across the North Pole, although its origin here is shifted from the Laptev Sea cell to the Central Arctic cell. At any particular time, the Ekman velocity u_e at the surface can be as large or larger than the geostrophic velocity u_g at the surface. However, over longer timescales the geostrophic component of velocity tends to dominate. Figure 2 shows all of the positions of Levitus data within our domain, divided by season. The data are obviously sparse in the eastern Arctic, which casts some doubt on the calculated geostrophic velocities (Figure 1) in this region. A sensitivity study is described in section 4.2.2 below in which intercell transports are eliminated completely in favor of climate damping.

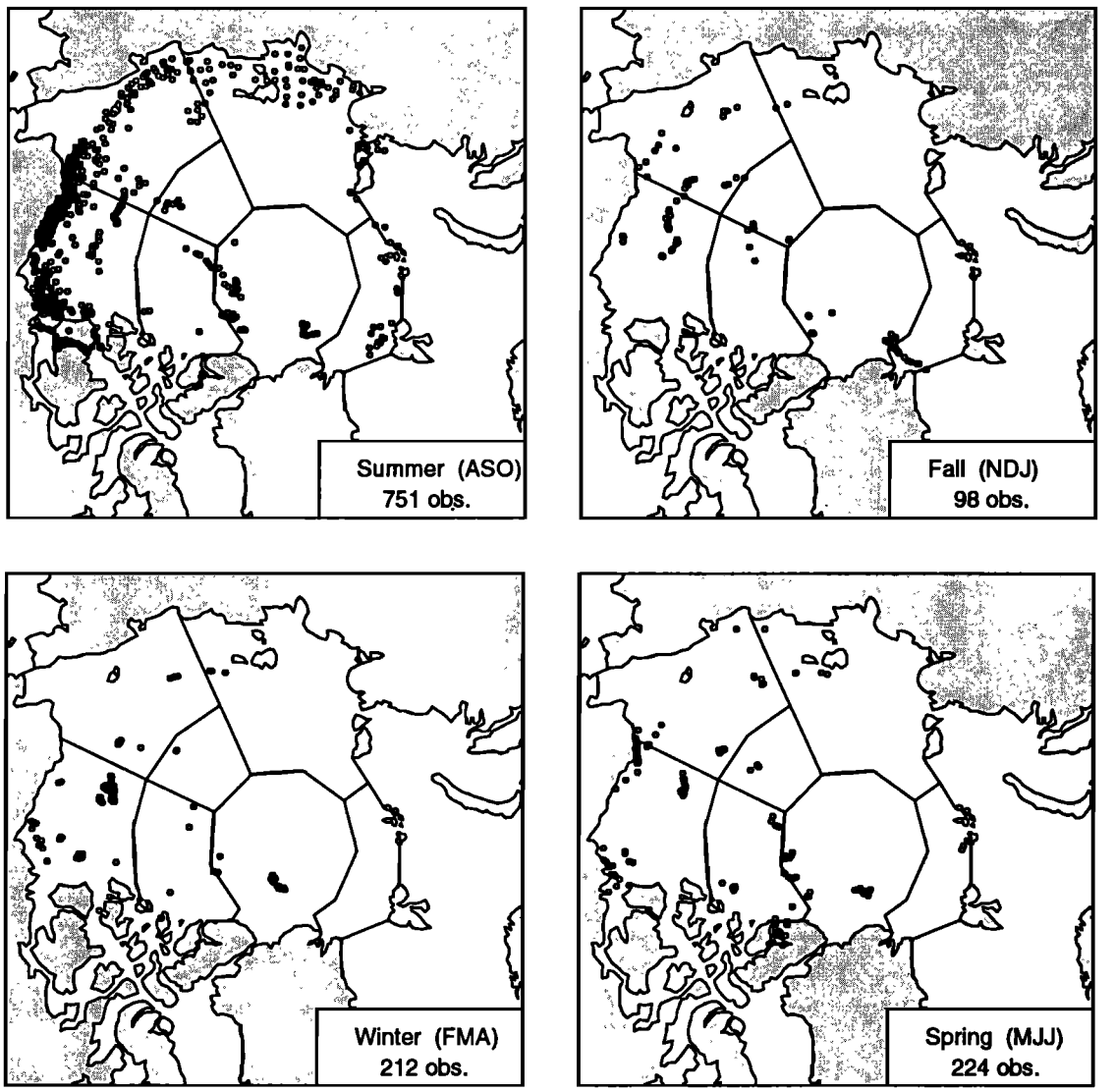

Figure 2. The locations of Levitus data within the seven-cell domain, presented by the seasons defined in the data set. Most data are from the summer, when the ice cover is at a minimum and surface salinities are low.

2.3. External Boundary Conditions

Conditions on the external boundaries are determined as follows. Outflow occurs at Fram Strait within the East Greenland Current (from the Nansen Basin cell) and within the Canadian Archipelago (from the Beaufort Sea, Canada Basin, and North Pole cells). The velocities here are calculated by the method of *Björk* [1989], in which we assume geostrophic outflow confined by a boundary on the right (looking downstream) which enters an ambient pool of constant density water. The ambient density is that of the outflowing cells' density at the fixed level of no motion, which is taken to be 200 m (the deepest level of the ocean model) in the East Greenland Current and in the outflow from the North Pole cell through Nares Strait, and is 150 m in the outflows from the Beaufort Sea and Canada Basin cells (due to shallow bathymetry there). Thus the outflow velocities vary at each time step and are (individually) unconstrained by any overall balance requirements.

Inflow occurs at Bering Strait and from the Kara Sea into the Laptev Sea. (The inflow of salty water in the West Spitsbergen Current is neglected here, since its freshwater content is very small [*Aagaard and Carmack*, 1989], and it tends to subduct below the bottom level of our model at 200 m.) Again, we follow the method of *Björk* [1989], assuming that a given volume of water flows into the downstream cell at its neutral density level. The inflow at Bering Strait is assumed to vary sinusoidally through the year, with a mean of 0.8 Sv and an amplitude of 0.4 Sv [*Coachman and Aagaard*, 1988]. The associated salinity is also assumed to vary sinusoidally, with a mean of 32.2 ppt and an amplitude of 0.6 ppt [*Björk*, 1989]. The maximum in the volume flux occurs in late summer and is coincident with the minimum in salinity.

The volume flux from the Kara Sea into the Laptev Sea represents flow through Vilkitsky Strait and between Franz Josef Land and Severnaya Zemlya, and is roughly 0.64 Sv [*Pavlov and Pfirman*, 1994]. This water is the product of mixing between the fresh water from the Ob, Yenesey, and other rivers and the relatively salty water of North Atlantic origins that has entered the Kara from the Barents Sea. Its bulk salinity is 31.76 ppt, which we calculate as follows. Table 3 shows a freshwater budget for the Barents and Kara Seas, which uses the data by *Aagaard and Carmack* [1989]. The table shows a surplus of fresh water, which we assume flows in liquid form into the Arctic Ocean with the volume flux just mentioned (0.64 Sv). Then the salinity is determined by the relationship between freshwater and volume fluxes, which is defined by (5) in section 4 below.

The Bering Strait water is heavy enough that it always enters the Chukchi Sea below the bottom of the mixed layer. The Kara Sea water is sometimes light enough to enter the surface waters of the Laptev Sea during winter, but most often lies just under the mixed layer.

2.4. Ocean Surface Fluxes

The ocean surface boundary condition for salinity is the sum of fluxes from ice melt minus growth (*MG*), from river runoff (*R*), and from net precipitation minus evaporation (*PE*). The first of these is derived via the parameterization described in TRMS, and includes the effects of ice growth, melt, and brine drainage.

We calculate the river runoff as follows. The runoff into the Beaufort Sea, averaging 290 $km^3\ yr^{-1}$, is estimated from daily flow rates for the MacKenzie, Peel, Arctic Red, Anderson, Babbage, Big, British, and Clifton Point rivers (measurements provided by the Water Resources Branch, Inland Waters Directorate, of the Water Survey of Canada). The Kolyma is the only major river draining into the Chukchi Sea cell; it has a mean runoff of 72 $km^3\ yr^{-1}$. For our Laptev Sea cell, the major rivers are the Lena, Indigirka, Yana, Olenek, and Katanga rivers, which together provide a mean runoff of 710 $km^3\ yr^{-1}$. The Siberian river data, in the form of monthly values for the years 1958–1988, were obtained under a cooperative agreement between the Office of the Chief Hydrologist, United States Geological Survey and its Russian counterpart. The data were provided by H. Lins, Office of the Chief Hydrologist, U.S. Geological Survey. The runoff is treated in the model as an ocean surface salinity flux over the area of the cell into which it flows.

For all cells we use a central Arctic monthly climatology of *PE* from *Vowinckel and Orvig* [1970]. We assume that the September through June snow fall, totaling 6.66 cm water equivalent, all melts and drains into the ocean at the start of summer. The model summer begins when buoy temperatures reach zero and the SMMR data show the first indication of open water, which varies from year to year and from cell to cell but is generally in early to mid June. The 1.73 cm of *PE* during July and the 0.81 cm during August are assumed to enter the ocean directly.

The resulting freshwater fluxes at the ocean surface are shown in Figure 3 for each region and for the Arctic Ocean as a whole. Positive values indicate a freshening effect, while negative values mean a salinification. The gray represents the fluxes due to *MG*, while the black represents the combined effects of *R* and *PE*. In each panel, the mean total flux is noted in the lower left corner;

Table 3. Freshwater Budget for the Barents and Kara Seas From *Aagaard and Carmack* [1989] Assuming No Exchange With the Arctic Ocean

Source, Sink	Transport, Sv	Yield, cm yr^{-1}
Precipitation minus evaporation	0.009	10
River runoff	0.057	67
Norwegian Coastal Current	0.008	10
Atlantic water inflow to Barents Sea	-0.017	-21
Net	0.056	67

Positive values indicate freshening. The area of the Barents and Kara seas is $2.63 \times 10^6\ km^2$.

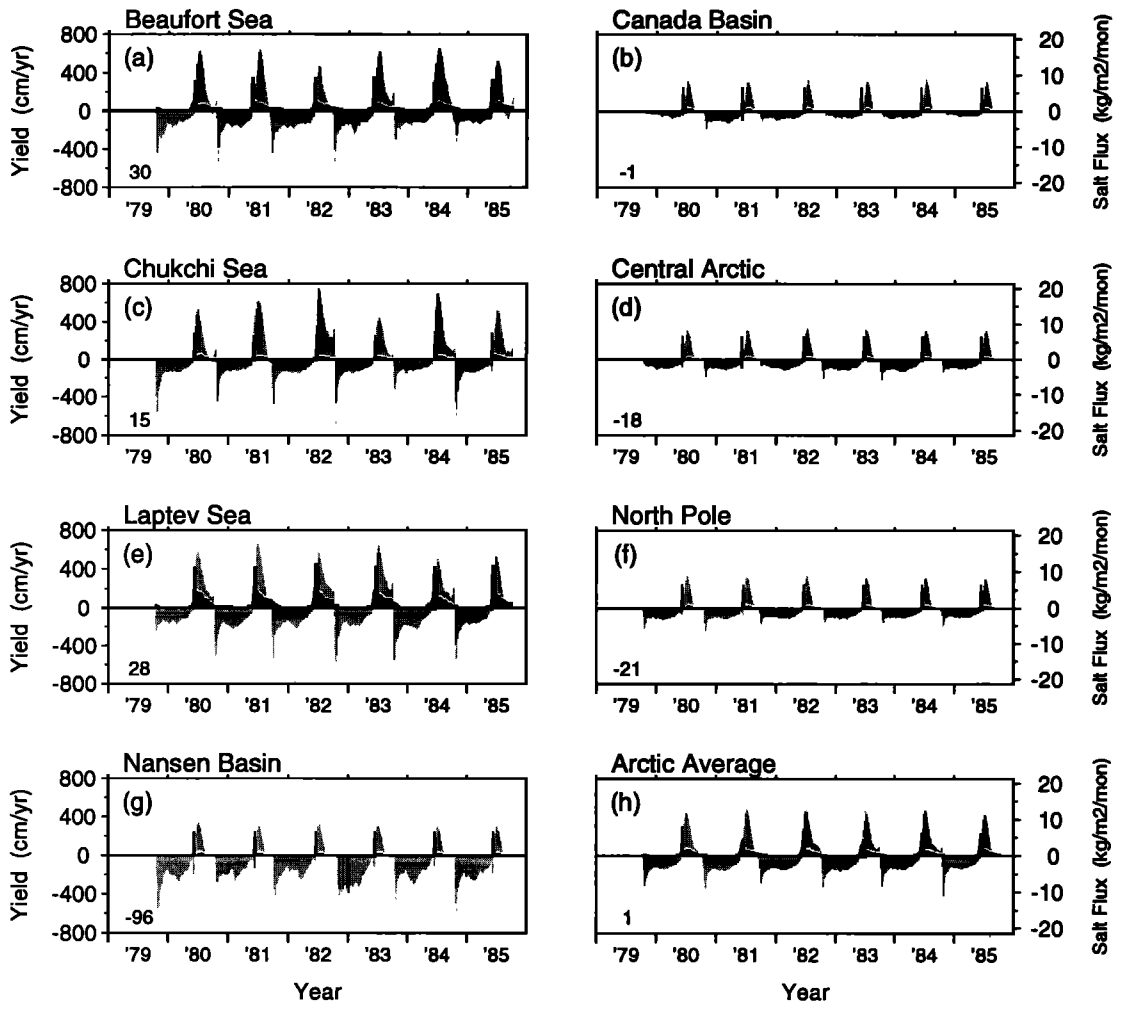

Figure 3. The surface freshwater flux in each cell (cm yr^{-1}) due to ice melt minus growth (gray) and to the combined effects of river runoff and net precipitation minus evaporation (black). Positive means a freshening, while negative means a salinification. The mean total flux is given in the lower left of each panel, and shows net freshening in the Beaufort, Chukchi, and Laptev seas and net salinification in the other cells. There is very little net effect over the Arctic as a whole (Figure 3h). The equivalent salt flux (kg m^{-2} $month^{-1}$) is also shown for comparison with *Thomas et al.* [this issue].

individual means for *R*, *PE*, and *MG* are given in Table 4. The Beaufort, Chukchi, and Laptev seas all receive a net freshening flux, while the other cells receive a net salinification. There is net ice growth in all regions except the Chukchi, where there is net melting of 0.4 cm yr^{-1}. There is strong ice growth in the Nansen Basin, of nearly 1 m yr^{-1}. The average of all these fluxes over the entire domain (panel h) is essentially zero, showing that *R* and *PE* fluxes are balanced by *MG*.

River runoff enters the Beaufort, Chukchi, and Laptev seas, reaching a maximum in early summer but remaining nonzero throughout the year. Precipitation minus evaporation is greatest at the beginning of summer owing to snow melt. The *MG* flux has a large negative peak during fall freeze-up, a smaller negative peak at the beginning of summer due to brine drainage, and a large positive peak at melt onset. In early summer, the (positive) peak due to snow melting occurs simultaneously with the (negative) peak due to brine drainage (panels f and g). The fluxes due to *MG* are generally much larger than those due to *R* or *PE*. This would not be the case if our model had high resolution near each river mouth, where the runoff is often confined close to shore [*MacDonald et al.*, 1989].

2.5. Initial Conditions and Numerical Details

The salinity profiles are initialized with the Levitus data from summer, averaged into the seven cells. Levitus data from the other seasons in the Arctic are quite sparse (Figure 2). (The initial salinity profile in the Nansen Basin is set equal to that in the North Pole cell, because the Levitus data in the Nansen Basin during summer are biased, coming exclusively from within the West Spitsbergen Current.) The resulting profiles exhibit essentially no mixed layer in any of the cells. The model equilibrates slightly faster if we create a mixed layer in each cell by imposing an initial "spin up" of 90 days during which the surface freshwater flux is -200 cm yr^{-1} and the ocean surface stress is 0.1 N m^{-2}.

The salinity and momentum equations are integrated on a vertical grid of 5 m uniform spacing within each cell, from the surface to 200 m depth. The grid is staggered with respect to variables and their fluxes. Leapfrog time differencing is used, with a 1-hour time step. On each boundary, the vertical viscosity coefficient calculated by the Mellor-Yamada model in the neighboring cells is averaged and used to calculate the velocity profile forced by the ice stress across that boundary. The horizontal advection of salinity into each cell is then calculated by upstream differencing.

Table 4. The Model-Derived Mean Freshwater Budget for Each Cell in Terms of Yield

Cell	R	PE	MG	AO	W	Y_O	AI	Y_I
Beaufort Sea	30	9	-9	-39	20	11	-1	8
Chukchi Sea	6	9	0	87	-95	7	13	13
Canada Basin	0	9	-10	32	-18	13	-16	-6
Central Arctic	0	9	-27	0.4	29	11	-23	4
Laptev Sea	45	9	-26	-28	4	4	-31	-5
North Pole	0	9	-30	16	2	-3	-27	3
Nansen Basin	0	9	-105	200	-91	13	-99	6
Arctic Ocean	16	9	-24	26	-21	6	-21	3

Yield is in cm yr^{-1}, where R is river runoff, PE is net precipitation minus evaporation, MG is net ice melt minus growth, AO is net ocean freshwater transport, W is up/downwelling of freshwater, and AI is net sea ice freshwater transport. Positive values indicate freshening. The net yield in the ocean is defined as $Y_O = R + PE + MG + AO + W$, while the net yield in the ice is defined as $Y_I = AI - MG$. Yields have been calculated using an Arctic Ocean area of 6.92×10^6 km^2.

Other boundary conditions for the ocean model are as follows. The salinity at the bottom of the domain at 200 m depth is fixed at its initial value. This allows the net up/downwelling within each cell to provide a salinity flux at this boundary. The surface momentum flux on the boundaries is provided by the ice motion, as discussed in section 2.2. Within each cell, we impose a constant 0.08 N m^{-2} at the surface. (We did not use cell-average stresses from the ice motion, since this produced very weak mixing which we attribute to the large-scale averaging of velocity (TRMS).)

The model is run for four cycles of 6 years each, where each cycle begins on October 1, 1979, and ends on September 30, 1985. The model equilibrates by the second cycle; results are shown from the fourth cycle.

3. Results

The model predicts mixed layer depths that vary seasonally, with a gradual deepening during the winter and a more abrupt shoaling in early summer. The three cells with riverine influence (Beaufort, Chukchi, and Laptev seas) have mixed layer depths that vary between about 5 m in summer to 25 m in winter. Other cells' mixed layers are generally deeper by about 5 m throughout the year, except for the Nansen Basin mixed layer, which deepens to 50-100 m in winter owing to the large negative freshwater fluxes (Figure 3) and low stratification there.

3.1 Mixed Layer Salinity

Figure 4 shows the mixed layer salinity (MLS) time series for the seven cells plus the Arctic average integration. The mean MLSs are given in the lower left corner of each panel in Figure 4. They show a relatively fresher western Arctic and a more saline eastern Arctic. The Nansen Basin is the saltiest region, reflecting the influence of high ice growth rates (Figure 3g). In Figure 4h, the solid line shows the area-weighted average from the seven individual cells, while the dashed line shows the result from the "one-dimensional" Arctic average simulation. The difference is due to non-linearities in the response of the mixed layer to buoyancy and momentum fluxes at the surface. Specifically, in the "one-dimensional" simulation, the early summer freshwater fluxes are spread out over a large area and thus do not cause as much mixed layer shoaling as when they are applied to more localized areas. Thus the one-dimensional simulation overestimates the average MLS by about 0.7 ppt in our study. The (area-weighted) average MLS in Figure 4h is 30.58 ppt.

The seasonal cycle is most pronounced in the Beaufort, Chukchi, and Laptev seas. This is due to (1) summer riverine inputs and to (2) a larger seasonal cycle of melting and freezing that occurs at lower latitudes. We suspect that the seasonal cycle is somewhat overestimated due to the interpretation of river runoff as a surface flux to be distributed over a large area. The weakest seasonal cycle occurs in the Canada Basin, where there is a small melt/freeze signal, no river inputs, and a long path from the fresh water sources along the mean circulation pattern (Figure 1).

In Figure 5 we compare the seasonal cycle of MLS in our model with previous models and limited observations in three regions: the Beaufort Sea, the Canada Basin, and the Arctic Ocean average. The model's average seasonal range in the Canada Basin is 30.9-31.5 ppt, which may be compared with a range of 31.25-31.65 ppt observed at ice island T-3 in this area during 1970-1973 [*Morison and Smith*, 1981]. In the Beaufort Sea, the model predicts an average range of 28.7-31.3 ppt, which may be compared with AIDJEX observations during the 1975-1976 winter of 29.8-31.1 ppt (raw) or 29.8-30.5 ppt (detrended) [*Lemke and Manley*, 1984]. The AIDJEX observations probably reflect more "interior" conditions than our Beaufort Sea cell represents. Thus we also compute the seasonal range for an areal average of the Beaufort Sea and Canada Basin cells, which is 29.6-31.4 ppt and more nearly agrees with the raw AIDJEX observations. Finally, the Arctic average (Figure 4h, solid line) has a seasonal range of 29.6-31.5 ppt, which may be compared with previous model estimates of 30-32 ppt [*Björk*, 1989], 30.7-31.5 ppt [*Mellor and Kantha*, 1989], and 30.5-31.8 ppt [*Häkkinen and Mellor*, 1990].

There is significant interannual variability in some regions. Comparison with Figure 3 indicates that this is driven primarily by the surface buoyancy forcing. For example, the weak melt in the

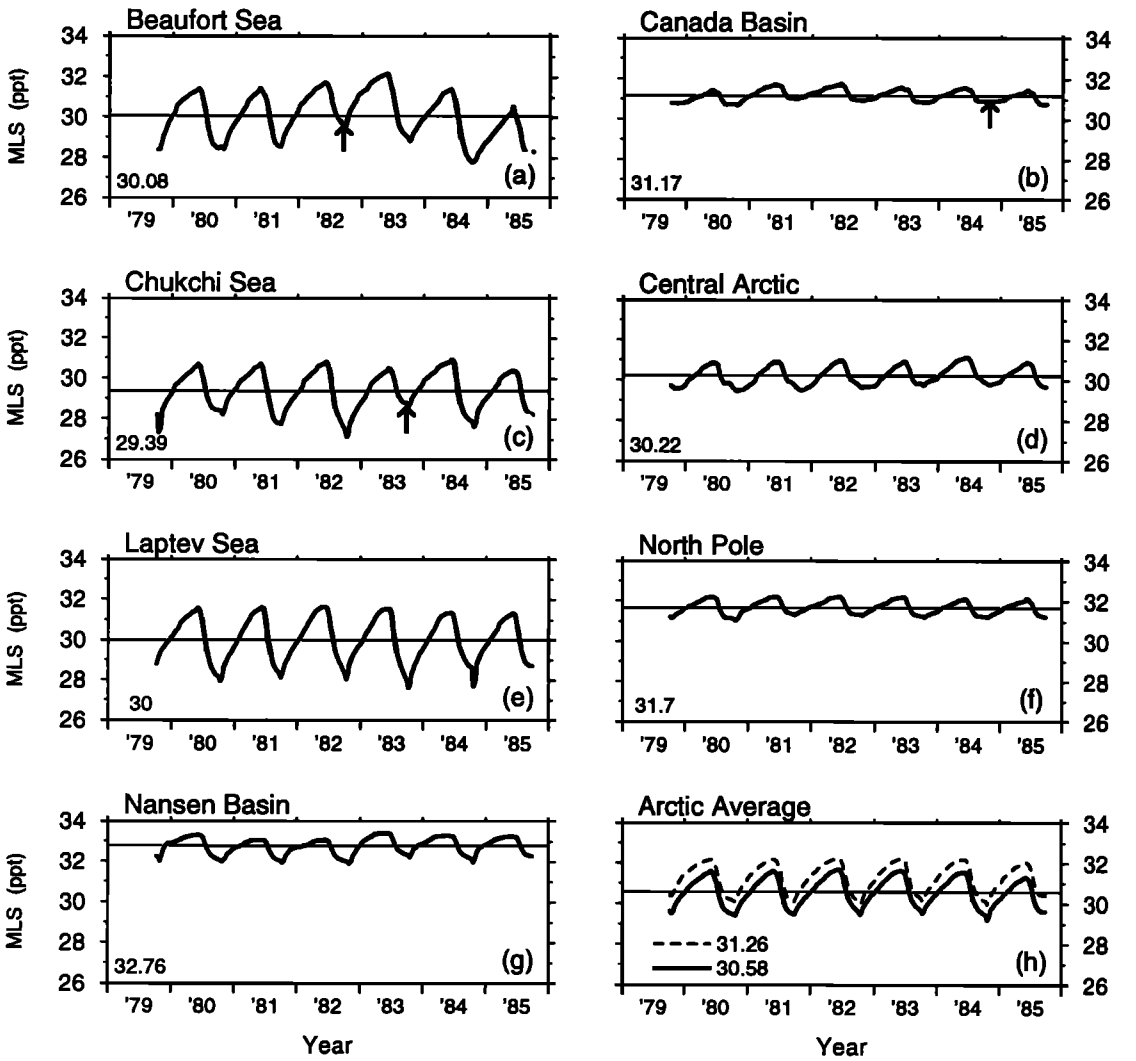

Figure 4. The mixed layer salinity (MLS) in each cell (ppt), with the mean value given in the lower left. The greatest seasonal cycle occurs in the Beaufort, Chukchi, and Laptev seas. The dashed line in Figure 4h shows the result of a simulation in which the Arctic Ocean is treated as a single horizontally homogeneous cell, while the solid line in Figure 4h is simply the area average of MLS in each of the seven cells. The "single-cell" simulation overestimates the mean MLS by about 0.7 ppt. The meaning of the arrows in Figures 4a – 4c is described in the text.

Beaufort Sea during 1982 (Figure 3a) leads to a relatively saline summer mixed layer in that year (Figure 4a). The difference in MLS between the two successive summers of 1981 and 1982 in the Beaufort Sea is an impressive 1.1 ppt. On the other hand, the weakest interannual variability is found in the North Pole cell, where the annual mean MLS over the 6 years varies from a minimum of 31.65 ppt to a maximum of 31.78 ppt. The biggest change in this cell from one year to the next occurs in 1983-1984 when the annual average MLS decreases 0.09 ppt, while the smallest change occurs in 1984-1985 and amounts to a decrease of only 0.002 ppt.

The MLS anomaly in the Beaufort Sea shows up in the Chukchi Sea by the following summer of 1983, and appears as a weak anomaly in the next summer of 1984 in the Canada Basin. The anomalies are noted by arrows in Figure 4. The advection of salinity anomalies in the Arctic has been noted by *Häkkinen* [1993] as a possible origin for salinity anomalies observed in the North Atlantic. The time series in this study are, unfortunately, too short for a more definitive diagnostic examination.

The interannual variability evident in individual cells is conspicuously lacking in the Arctic average time series. This is similar to the results of *Parkinson* [1991], who found that the interannual variability of sea ice coverage could be large in selected regions while small for the Arctic as a whole. The idea is that large climate signals in one part of the Arctic may be compensated by equal and opposite ones in another part. We explore this notion with respect to the outflow of freshwater from the Arctic Ocean in section 4.2.2.

The interannual variability of Arctic MLS has been shown by *Manabe et al.* [1991, 1992] and *Manabe and Stouffer* [1994] to be a particularly sensitive indicator of climate change. In their simulations, increases in atmospheric CO_2 lead to an increasing excess of precipitation over evaporation in high northern latitudes, enhancing the freshwater fraction in the already fresh Arctic Ocean. The magnitude of the freshening is about 0.01 ppt yr^{-1}, which is generally much less than the interannual variability seen in Figure 4. The variability of regional MLS from one year to the next in Figure 4 can be as much as 100 times the predicted trend from increasing atmospheric CO_2. Even in the North Pole cell, it would take at least 10 years of observations to separate a signal of 0.01 ppt yr^{-1} such as predicted by Manabe and coworkers from the noise of "normal" interannual variability.

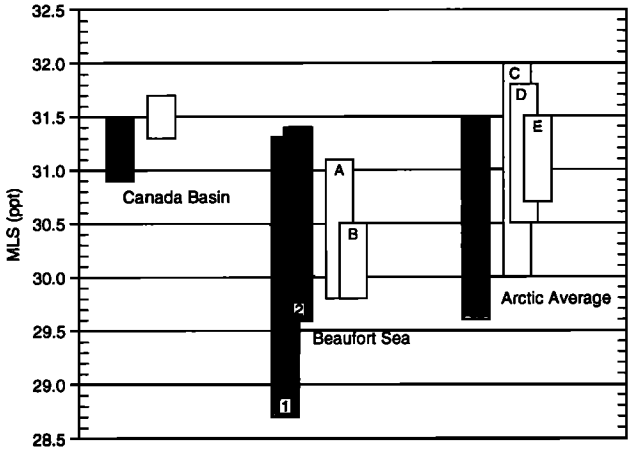

Figure 5. Comparison of the mean seasonal range of MLS from our model (dark bars) with observations and other models (light bars). The Canada Basin is compared with observations from the drifting ice island T3 [*Morison and Smith*, 1981]. The Beaufort Sea is compared with observations from AIDJEX [*Lemke and Manley*, 1984]. As discussed in the text, bar "1" represents the Beaufort Sea, while bar "2" represents an average of the Beaufort Sea and the Canada Basin. Also, bar "A" represents the raw observations while bar "B" denotes the detrended range. The Arctic average (solid curve in Figure 4h) is compared to model results from *Björk* [1989] (denoted "C"), *Häkkinen and Mellor* [1990] (denoted "D"), and *Mellor and Kantha* [1989] (denoted "E").

3.2. Volume Transport

Figure 6 shows the annual average volume transport across each boundary. In the interior, transports are largely driven by the geostrophic velocities. (Ekman transports are significant in the upper 50 m.) The transports on the exterior inflow boundaries are fixed, while those on the exterior outflow boundaries vary depending on the stratification in the outflow cells. A comparison of inflows and outflows reveals the following.

1. For the domain as a whole, the total inflow is 1.4 Sv, while the total outflow is 1.1 Sv; the difference is provided by downwelling. For comparison, previous estimates of the total outflow in the upper 200 m are 1.0 Sv [*Björk*, 1989], 1.6 Sv [*Rudels*, 1987], and 3.5 Sv [*Stigebrandt*, 1981].

2. For Fram Strait, the outflow of 0.57 Sv is low compared to the estimate of 1.0 Sv by *Foldvik et al.* [1988] (and used by *Aagaard and Carmack* [1989]) for the outflow of Polar Water, which as defined in those studies occupies roughly the same vertical domain as our model, that is, the upper 200 m.

3. For the Canadian Archipelago, the outflow of 0.5 Sv may be compared to the estimate of 0.7 Sv determined by *Rudels* [1986] from matching an assumed geostrophic outflow (such as used in our model) with a balance model for Baffin Bay hydrography. *Aagaard and Carmack* [1989] use a value of 1.7 Sv, citing a study by *Fissel et al.* [1988]. This is obviously a point of some uncertainty in the circulation of Arctic waters, which is unfortunate given its important role in the freshwater budget (Section 4).

4. The Arctic-average downwelling amounts to a weak 0.03×10^{-6} m s^{-1}, or 90 cm yr^{-1}. For comparison, *Wallace et al.* [1987] calculated an average downwelling of 100 cm yr^{-1} using a very different physical/chemical balance model. Also, the nearly global mean field of upwelling/downwelling computed by *Oort et al.* [1994] shows downwelling of $0\text{-}1\times10^{-6}$ m s^{-1} in both the North Pacific and North Atlantic Oceans; the Arctic Ocean itself was excluded from their study. Figure 6 shows the up/downwelling transport at 200 m depth within each cell. Broadly speaking, upwelling in the Laptev Sea is balanced by downwelling in the Chukchi Sea, Canada Basin, and Nansen Basin cells. A higher-resolution model would presumably also predict some downwelling within the Beaufort Gyre, centered near the point of intersection between the four western Arctic cells.

4. The Freshwater Balance

In keeping with estuarine nomenclature, we define freshwater as a measure of buoyancy, using salinity as a good approximation for density in the cold Arctic Ocean. The storage of freshwater H_{fresh} in the upper 200 m of the ocean is given by

$$H_{\text{fresh}} = \int_{-200}^{0} (S_{\text{ref}} - S)/S_{\text{ref}}\, dz \tag{4}$$

where, following *Aagaard and Carmack* [1989], we define $S_{\text{ref}} \equiv 34.8$ ppt. Then the freshwater transport M_{fresh} is given by

$$M_{\text{fresh}} = L \int_{-200}^{0} u\,(S_{\text{ref}} - S)/S_{\text{ref}}\, dz \tag{5}$$

where u is the velocity perpendicular to a boundary segment of length L. With these definitions, there is no freshwater if $S = S_{\text{ref}}$. Also, the freshwater flux is equal to the volume flux if $S = 0$, as is the case with river runoff. The definitions of H_{fresh} and M_{fresh} are similar for sea ice, except that a thickness-average S_{ice} is used in place of $S(z)$. (The definition of freshwater transport used by *Wijffels et al.* [1992] can be recovered from (5) by setting $S_{\text{ref}} \equiv 1000$ and multiplying the right hand side by the seawater density ρ, so that M_{fresh} becomes the water (H_2O) component of the sea water mass flux.)

The units of M_{fresh} are volume per unit time. River and estuarine studies generally use cubic kilometers per year, while oceanographic studies use Sverdrups ($\equiv 10^6$ m^3 s^{-1}). It is also fairly

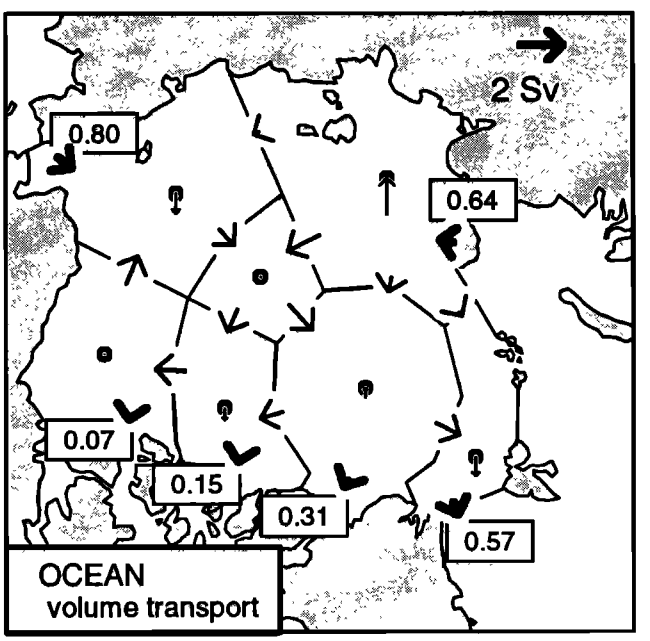

Figure 6. The mean oceanic volume flux (in sverdrup) across cell boundaries in the upper 200 m of the Arctic Ocean. The magnitudes of the inflows (from the Bering Strait and the Kara Sea), and the outflows (through the Canadian Archipelago and Fram Strait) are shown explicitly (boxes). The net upwelling/downwelling flux in each cell (using the same scale) is also shown.

common to consider the "yield" of riverine flow, in cm yr^{-1}, which is the volume flux divided by an outflow area. In this paper we will use both Sv and cm yr^{-1} for transport M_{fresh}, while the freshwater storage H_{fresh} will be given in meters.

To convert H_{fresh} and M_{fresh} from one reference salinity $S_{ref\text{-}1}$ to another $S_{ref\text{-}2}$, one may use the formula

$$[H_{fresh}, M_{fresh}]_2 = (1-\alpha)\,[H, M] + \alpha\,[H_{fresh}, M_{fresh}]_1 \quad (6)$$

where $\alpha \equiv S_{ref\text{-}1}/S_{ref\text{-}2}$, H is depth, and $M = L\int(udz)$ is volume flux. For example, *Aagaard and Carmack* [1989] use $S_{ref} \equiv 34.8$ ppt for the Arctic Ocean, and $S_{ref} \equiv 34.93$ ppt for the Greenland-Iceland-Norwegian (GIN) Sea. The difference in freshwater storage H_{fresh} using the two different reference salinities is negligible for the sea ice and zero for the purely fresh components (i.e., river runoff and precipitation minus evaporation), while it is about 10% for the seawater components (assuming $H = 200$ m and $H_{fresh} \cong 8$ m).

4.1. Climatology

Figure 7 shows the mean freshwater horizontal transports and storage in the sea ice and upper ocean. Clearly, there is more freshwater in the western Arctic than in the eastern. The mean ice transport carries this out Fram Strait, while the ocean circulation exports it out both Fram Strait and the Canadian Archipelago. The main points illustrated by this figure are given below.

1. The Arctic total freshwater storage in the sea ice is 2.4 m, or 16,000 km^3 over our domain. The corresponding oceanic storage is 7.7 m, or 53,000 km^3.

2. The total freshwater outflow in the upper ocean (0.063 Sv) is roughly 20% greater than that in the ice (0.051 Sv).

3. The freshwater inflows from the Bering Strait and the Kara Sea are the same to within 10%.

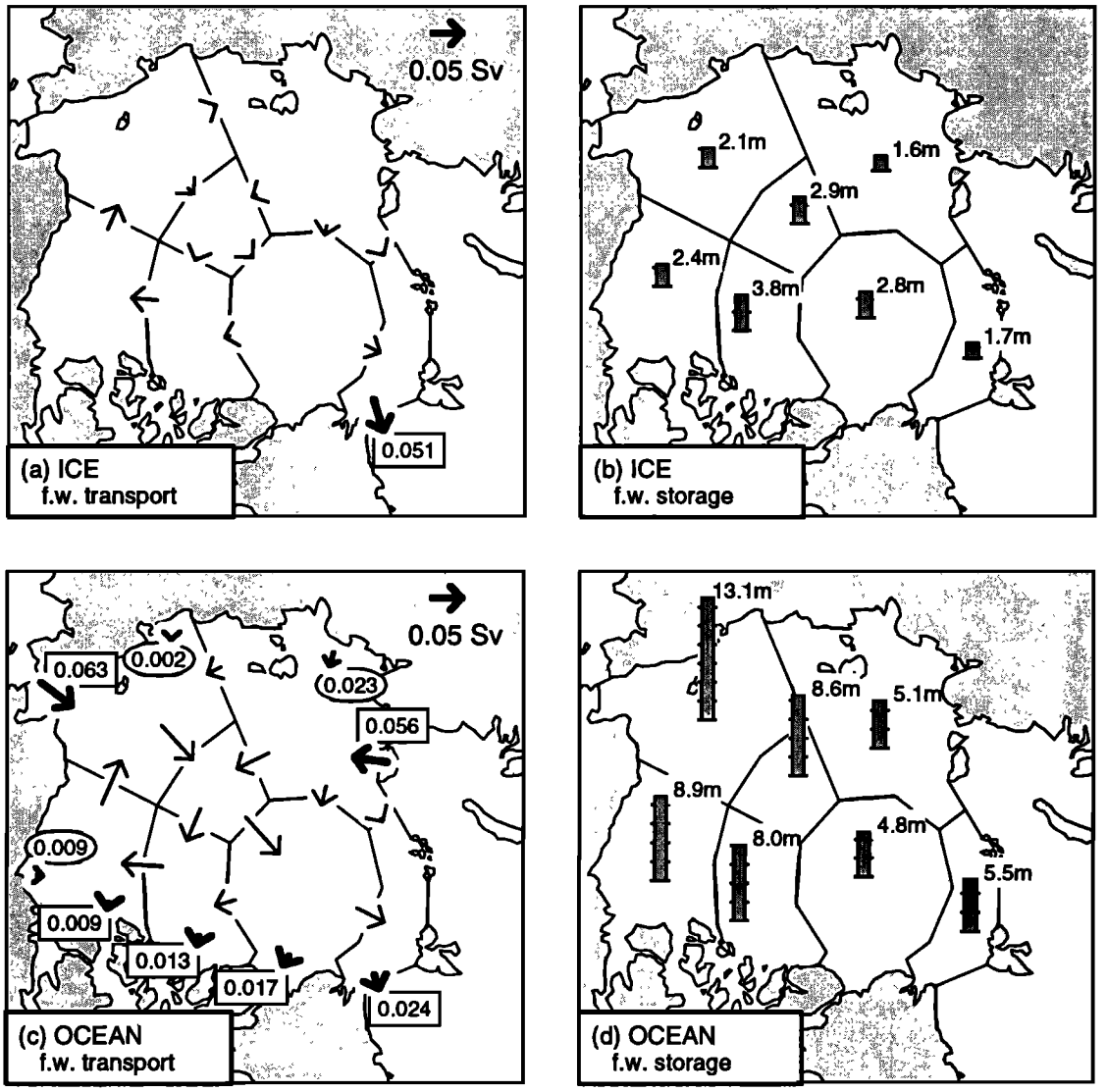

Figure 7. As in Figure 6, but for freshwater transport (in Sv) and freshwater storage (in meters) in the sea ice (Figures 7a and 7b) and in the ocean (Figures 7c and 7d)), respectively. The inflow and outflow values in Figures 7a and 7c are given explicitly (boxes), as are the river inflows (ovals). The total freshwater outflow from the Arctic Ocean is about 0.114 Sv, where 45% is sea ice flux through Fram Strait, 21% is oceanic flux through Fram Strait, and 34% is oceanic flux through the Canadian Archipelago.

4. The ocean transport of freshwater through Fram Strait is about 60% of that through the Canadian Archipelago (using the same reference salinity), even though the volume transports are about the same (Figure 6). This is not too surprising, given the fresher conditions in the western Arctic.

5. The ocean freshwater flow in the East Greenland Current (0.024 Sv) is a bit low compared to the value of 0.030 Sv estimated by *Aagaard and Carmack* [1989], while the total outflow through the Canadian Archipelago (0.039 Sv) is a bit high relative to their estimate (0.029 Sv). For Canadian Archipelago outflow, the discrepancy lies in the choice by *Aagaard and Carmack* [1989] of an average outflow salinity of 34.2 ppt, which seems high given the generally shallow sills in the archipelago. Our model-derived average outflow salinity from the three cells that drain into the Archipelago is 32.3 ppt (weighted by the geostrophic outflow transport) or 33.3 ppt (the simple depth average value). These bracket the value of 32.9 ppt determined by *Rudels* [1986] using a simple balance model for the Archipelago. Also, note that a smaller-scale examination of the freshwater budget of Baffin Bay might use a fresher reference salinity (*Rudels* [1986] found an average 200 m depth salinity in Baffin Bay of 34.0 ppt) which would lower the Canadian Archipelago freshwater flux to 0.027 Sv.

Table 4 presents the mean freshwater balance in each cell, and the (area-weighted) Arctic average. This balance may be expressed algebraically as

$$Y_O = R + PE + AO + W + MG \quad (7)$$

$$Y_I = AI - MG \quad (8)$$

where Y_O and Y_I are the net freshwater yields in the ocean and the ice, respectively, AO and AI are the horizontal advection of freshwater in the ocean and in the ice, respectively, and W is the vertical transport of freshwater at 200 m depth. The term W includes both vertical advection and vertical diffusion. The surface fluxes from rivers (R), precipitation minus evaporation (PE) and ice melt minus growth (MG) were discussed in section 2.4. In general, the regions with riverine influence (Beaufort, Chukchi, and Laptev seas) export liquid freshwater to the North Pole and Nansen Basin cells, where its fate is about equally distributed between ice growth and downwelling.

The overall freshwater budget in Table 4 (bottom row) shows the classic balance between the inputs of river runoff and precipitation minus evaporation and the output of net ice growth and export [e.g., *Aagaard and Greisman*, 1975]. Yet the budgets of the other cells demonstrate that these processes are not always colocated; for example, there is significant ice growth in the Nansen Basin where direct riverine influence is nil. Conversely, river runoff may mix to relatively deep levels close to shore and thus not be completely available for ice growth [*Hanzlick and Aagaard*, 1980]. Therefore the balance between net ice growth (MG) and river runoff (R) plus net precipitation minus evaporation (PE) that holds for the arctic as a whole is in fact easily violated on smaller scales.

The freshwater budget for the Arctic Ocean (Table 4, bottom row) indicates that about 40% (21 cm yr^{-1}) of the net inflow ($R + PE + AO$) downwells, freshening the layers below 200 m depth. *Aagaard et al.* [1981] estimate that 4 to 7 Sv of Atlantic Water enters the Arctic Ocean, with an average salinity of 35 ppt on entry and 34.9 ppt upon exit. This represents a freshening of 5-9 cm yr^{-1}, which if due solely to mixing with halocline waters would indicate that we are overestimating the freshwater downwelling flux. This may be true; however, *Aagaard et al.* [1981] note that the Atlantic layer also mixes with deeper, saltier water. This represents a sink of freshwater below the Atlantic layer which might partially balance our "excess" mixing from above. Further, Table 4 shows strong downwelling flux in the western Arctic, where the interface depth between halocline and Atlantic layers is probably deeper than 200 m, and thus more saline.

In Table 5 we provide a more detailed breakdown of the freshwater balance for the upper 200 m of the Arctic Ocean. For comparison, the estimates from *Aagaard and Carmack* [1989] are shown in the final column. The combination of river runoff and inflow from the Barents and Kara seas in our simulation approximately equals the river runoff in the work by *Aagaard and Carmack* [1989]. (Their domain included the Barents and Kara seas, into which river runoff is high.) Our model predicts less freshwater outflow in the form of ice than *Aagaard and Carmack* [1989] and about the same oceanic outflow.

A schematic plan view of the main terms in the mean freshwater balance is provided in Figure 8. Freshwater enters the Arctic Ocean from rivers, from the Bering and Kara seas, and from the net precipitation minus evaporation (the last is not shown in Figure 8). It exits through the Fram Strait and the Canadian Archipelago, downwelling along the way. We distinguish in the figure between the freshwater transport in the ocean and in the sea ice. There is a large amount of liquid (oceanic) freshwater transport on the Siberian side of the Beaufort Gyre, owing mostly to the inputs from the Bering Strait and Russian rivers. On the other hand, the Canadian edge of the gyre has a large sea ice component owing to the transport of thick multiyear ice from the Canada Basin (see also TRMS). The downward transport of freshwater occurs mainly in the Chukchi Sea and the Nansen Basin, as shown by the solid arrows. The dashed arrow in the middle of the Beaufort Gyre denotes the downward transport that is not resolved by our model but which presumably exists due to Ekman convergence. By the time the main transport reaches Fram Strait, sea ice is the dominant component, mainly because of high southward ice velocities. Of course, our model provides only a very low resolution picture of this circulation. Thus it does not resolve the detailed physics of river outflow near each river mouth, nor the subsequent small-scale flows that bring this water both off the shelf and along the coast, for example in the Siberian Coastal Current.

4.2. Interannual Variability

4.2.1. Arctic average. Figure 9 shows the time histories, for the Arctic Ocean as a whole, of the same freshwater terms as in Table 4. In each panel, the mean value is given in the lower left corner, while the running 1-year mean is shown as a dashed line. The ice storage term (Figure 9a) shows evidence of a multiyear cycle, with an annual-average minimum in 1982 that is about 10% lower than in 1980 or in 1985. The ocean storage term (Figure 9b) shows much less interannual variability. The amount of freshwater in the upper 200 m of the Arctic Ocean is about 3 times that in the overlying sea ice (although this is somewhat sensitive to the choice of reference salinity; see (6)).

The total river inflow is fairly constant from year to year, although the shapes of the peaks in Figure 9g do vary. The precipitation minus evaporation term (Figure 9h) is constant when integrated over each year; the different heights and widths of the peaks are due to variations in the beginning of summer for the different cells (section 2.4).

The multiyear cycle in the sea ice storage term (Figure 9a) is determined by the balance between advection (Figure 9c) and net

Table 5. Model-Derived Mean Freshwater Budget for the Upper 200 m of the Arctic Ocean

Source, Sink	Transport, Sv	Yield, cm yr^{-1}	Yield,* cm yr^{-1}
Precipitation minus evaporation	0.020	9	9
River runoff	0.035	16	48
Inflow			
From Barents and Kara seas (Table 3)	0.056	25	--
Bering St.	0.063	29	25
West Spitsbergen Current	0.00	0	-3
From the Atlantic Ocean to the Barents Sea	--	--	-4
Outflow			
Fram Strait Ice	-0.051	-23	-40
East Greenland Current	-0.024	-11	-12
Canadian Archipelago	-0.039	-18	-14
Upwelling/downwelling	-0.046	-21	--
Net	0.014	6	9

All yields have been calculated using an Arctic Ocean area of 6.92×10^6 km^2 (i.e., excluding the area of the Barents and Kara seas). Positive values indicate freshening.

* The budget using the calculation of *Aagaard and Carmack* [1989].

melt minus growth (Figure 9e). As discussed in TRMS, ice mass is lost in the early 1980s because the net loss of ice through advection is greater than the net growth of ice within the domain. This situation reverses in the latter part of the simulation. The result is a minimum in ice mass (and thus in ice freshwater storage) in 1982. Note that we use the form of net ice advection (Figure 9c) appropriate for a basin-wide budget study, that is, we include the model-data adjustment terms discussed in Appendix B of TRMS.

Figure 9d shows that there is net import of freshwater in the ocean throughout the year, with a seasonal cycle that is forced primarily by the assumed sinusoidal inflow at Bering Strait. The resulting downward flux (Figure 9f) is sensitive to the net Ekman convergence within each cell, which is forced by sea ice advection (Figure 9c) and is thus relatively noisy. The interannual variability for these and the other freshwater fluxes to the ocean (Figures 9d-9h) is essentially nil. This is not true, however, for individual cells.

4.2.2. Outflows. Figure 10 shows the variation in annual average freshwater outflow from the Arctic Ocean. In Figure 10a we compare the outflows of freshwater in sea ice and in the upper ocean at Fram Strait. Both peak in the early 1980s. The variability is quite large in the sea ice component, and much less so in the ocean component, which makes up about a third of the total outflow. Figure 10a indicates that the interannual variability in the freshwater flux through Fram Strait is about 0.05 Sv, or 1560 km^3 yr^{-1} in the sea ice, and about an order of magnitude less in the ocean, for a total of about 1700 km^3 yr^{-1}. If sustained over a year, this outflow would be nearly sufficient to produce the freshwater anomaly (2000 km^3) that occurred during the "Great Salinity Anomaly" of the late 1960s to early 1970s [*Dickson et al.*, 1988; *Aagaard and Carmack*, 1989], in which GSDW formation was completely shut down.

If the freshwater outflow in Fram Strait peaks in the early 1980s, what happens in the Canadian Archipelago? Figure 10b shows the year-averaged variability of ocean freshwater outflow in both of these locations, where the Canadian Archipelago component consists of contributions from the Beaufort Sea, the Canada Basin, and the North Pole cells. The outflow through the Canadian Archipelago tends, in our model, to compensate the ocean outflow in the Fram Strait. This is seen more clearly in Figures 10c and 10d, which shows the ocean anomaly transports (6-year mean subtracted) for the Fram Strait and Canadian Archipelago, respectively. Fram Strait outflow anomalies seem to lead those in the Canadian Archipelago by one year.

These anomalies are admittedly quite small, relative to the means. Are they real? We performed the following sensitivity study to address this issue. The largest uncertainty in our model is probably the use of geostrophic velocities computed using the climatological Levitus data. In the sensitivity study, we eliminated all inter-cell advection ($u_e + u_g$) and parameterized it by damping the cell-average salinity profiles to climatology, using a 3-year time constant. This is in fact a common method for linking essentially one-dimensional "column" models to create a quasi-three-dimensional model [e.g., *Lemke et al.*, 1990; *Lascaratos et al.*, 1993]. The resulting freshwater transport anomalies are qualitatively similar to the standard case (Figures 10c and 10d, dashed lines) and are thus independent of the intercell transports.

What is producing this compensation effect between the two outflow channels? The anomalies shown in Figures 10c and 10d are highly correlated with MLS anomalies in Figure 4, via our

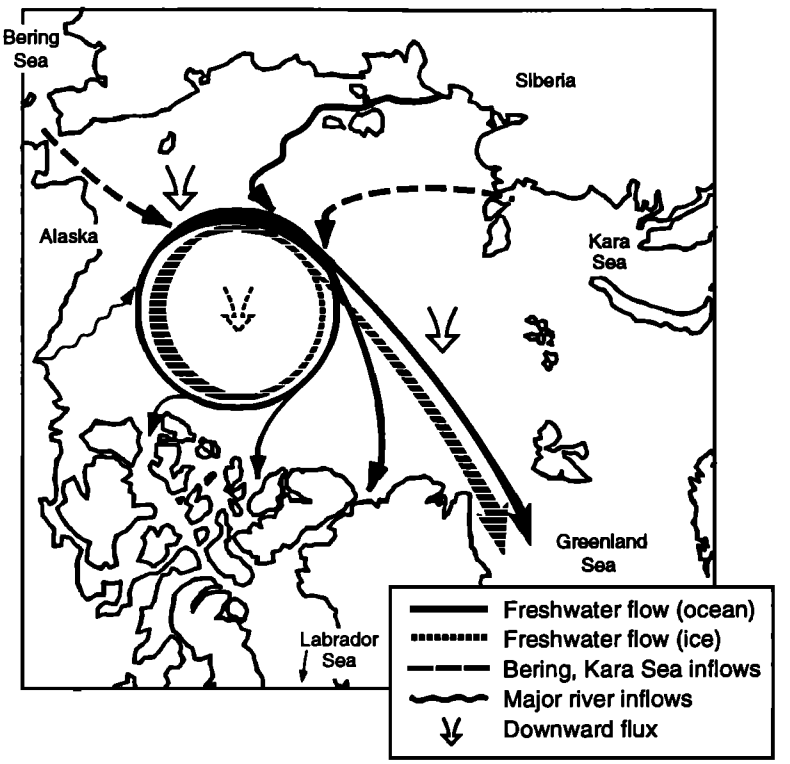

Figure 8. A plan view of our concept of the freshwater balance of the upper Arctic Ocean. Line thicknesses are qualitatively related to the magnitude of the fluxes. Freshwater enters the basin from river runoff, precipitation minus evaporation (not shown), and from the relatively fresh inflowing sea water in the Bering and Kara seas. It is concentrated in the western Arctic by the mean circulation, that is, the Beaufort Gyre and presumed westward flow along the Siberian shelf. Some of this freshwater downwells in the Chukchi Sea and in the center of the Beaufort Gyre, the latter not explicitly modeled here and thus indicated by a dashed arrow. The rest flows across the eastern Arctic, where there is additional downward flux that serves to freshen the relatively salty Atlantic Water layer that resides at several hundred meters depth. The bulk of the freshwater, however, continues across the Arctic Ocean and out into the Atlantic Ocean through Fram Strait and the Canadian Archipelago.

geostrophic outflow parameterization (section 2.3). Changes in these outflows create local changes in upwelling or downwelling, and since these are compensating, the domain-average upwelling/downwelling (Figure 9f) shows little variation. Most of the variability in Canadian Archipelago outflow comes from the Beaufort Sea cell. The MLS anomalies are in turn mostly a product of ice-ocean salt flux anomalies (Figure 3), which are provided by the ice model (TRMS). They are influenced by both thermodynamics and advection, although as discussed by TRMS, variability in the former may be underestimated. If this is so, then these anomalies could be largely forced by anomalous ice motion patterns. *Häkkinen* [1993] reached a similar conclusion with respect to the outflows from Fram Strait alone. The compensation effect shown in Figure 10 is small, however, and should be viewed as suggestive. A more definitive statement awaits a study with higher resolution and longer time series.

4.2.3. Increased CO_2 simulation. Finally, we discuss the results from a very simple "climate change" experiment. As noted in section 3.1, *Manabe et al.* [1991, 1992] and *Manabe and Stouffer* [1994] have predicted that the effect of increased atmospheric CO_2 would be to increase precipitation minus evaporation, and thus also river runoff, in high northern latitudes. The magnitude of these increases at 100 years into the simulation was estimated at 6 cm yr-1 for each of R and PE in the work by *Manabe et al.* [1991]. A simulation using our model was run using these additional freshwater inputs, which total 0.026 Sv over the Arctic Ocean. An important caveat, beyond the obvious one of using a very simple model, is that the ice component of this run was not changed from the control, since it is tied directly to satellite observations. However, *Manabe and Stouffer* [1994] found that the change in net ice melting was small in their simulation, compared to the increases in river runoff and precipitation minus evaporation.

As noted previously (Figures 7c and 10b) there is normally about 60% more liquid freshwater outflow through the Canadian Archipelago in our model as there is through the Fram Strait. The "climate change" simulation predicts a similar relationship for the CO_2-induced increases in freshwater outflows through the two channels. This means that the absolute magnitude of the increase in freshwater outflow through the Canadian Archipelago (about 0.014 Sv) is about 60% more than that through the Fram Strait (about 0.009 Sv). This makes sense, since freshwater storage tends to concentrate in the western Arctic owing to the mean circulation as well as the geographic distribution of source terms (Figures 7 and 8). We are led to speculate that increasing freshwater sources in a future CO_2-rich environment might enhance the stability of surface waters (and thus inhibit deep convection) in the northwest Atlantic more than in the northeast Atlantic.

5. Conclusions

The advantage of our study over standard ice-ocean models is that it uses assimilated satellite and buoy observations to derive surface salinity and momentum fluxes. The main disadvantage is

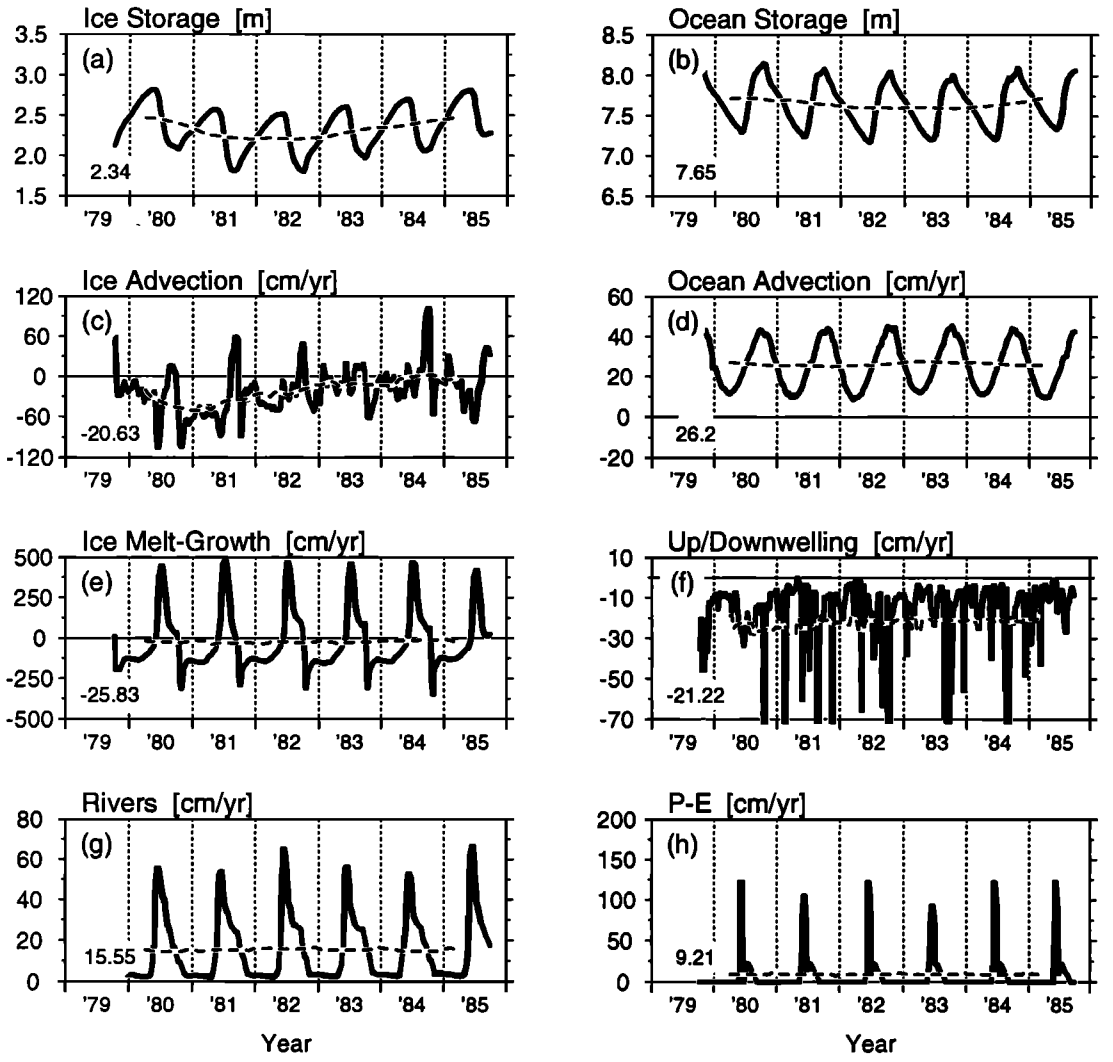

Figure 9. The time histories, for the Arctic Ocean as a whole, of the terms in the freshwater budget given in the bottom row of Table 4. Also plotted is the 1-year running mean (dashed line).

of course its low horizontal resolution since, while it allows us to concentrate on large-scale budget computations, it cannot capture the details of transport and exchange near fronts and boundaries. These details are better captured in fully three dimensional ice-ocean models. Even these models, however, generally do not resolve some of the first-order processes in the freshwater budget, such as the details of river outflow into ice-covered seas or the flow of freshwater through exceedingly narrow straits (Nares, Vilkitsky).

5.1. Mixed Layer Salinity Variability

There is substantial variability in MLS over the Arctic Ocean. The seasonal cycle is large (1-4 ppt in our simulation), and its amplitude varies tremendously with geographic region. The interannual variation in regional MLS can be as high as about 1 ppt yr^{-1} (and would undoubtedly be higher with higher spatial resolution). This variability is greatest near the low latitude coasts (Beaufort, Chukchi, and Laptev seas) where river runoff and sea ice melting play a large role. It is much reduced in the central parts of the Arctic Ocean, amounting to only about 0.05 ppt yr^{-1} in the North Pole cell. In Section 3.1 we note that *Manabe et al.* [1991] found MLS to be a parameter that is particularly sensitive to the effects of increasing atmospheric CO_2. Thus if we are to use MLS as a climate change indicator, our results serve as a reminder that trends in MLS will be much easier to detect in the central part of the Arctic basin than it will be closer to the coasts. However, our results also indicate that it will be difficult to detect a climate change signal of a magnitude predicted by *Manabe et al.* [1991] (about 0.01 ppt yr^{-1}) in any part of the Arctic Ocean until a decade or more of observations are made.

5.2. Freshwater Outflows

Our results indicate that there was a maximum in the freshwater outflow from the Arctic Ocean through Fram Strait during the early 1980s. This applies to both the solid (sea ice) and liquid (ocean) components, the latter of which constitutes about a third of the total transport in Fram Strait. Our results suggest that the liquid freshwater outflows to the northeast Atlantic Ocean (Greenland Sea) and to the northwest Atlantic Ocean (Labrador Sea) may be out of phase. A caveat is that Fram Strait is much closer geographically to the Greenland Sea than the Canadian Archipelago is to the Labrador Sea. Nonetheless, if freshwater transports have a (negative) influence on deep water formation, as suggested by *Aagaard and Carmack* [1989], then deepwater formation in the Greenland and Labrador Seas may be out of phase as well.

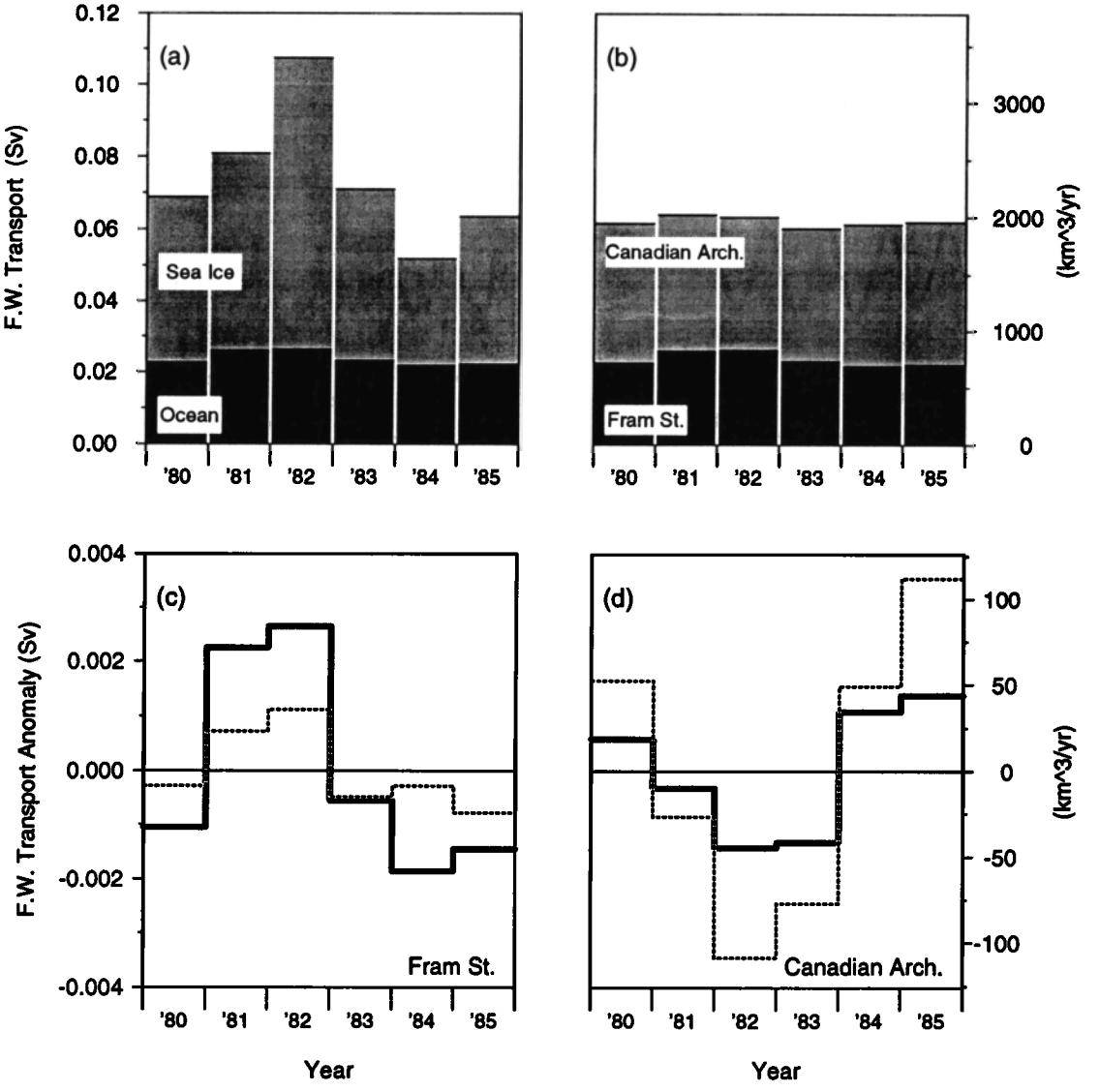

Figure 10. The variability of the annual average export of freshwater from the Arctic Ocean. (a) The export across Fram Strait in the ocean and in the sea ice. The oceanic component constitutes about a third of the total export. (b) The total ocean export in the Fram Strait and in the Canadian Archipelago (where the latter represents outflows from the Beaufort Sea, Canada Basin, and North Pole cells). (c) and (d) The yearly anomalies of oceanic transport in Fram Strait and the Canadian Archipelago, respectively, where the solid line represents the standard experiment and the dashed line represents the advection sensitivity study described in section 4.2.2.

Aagaard and Carmack [1989] cite *Fissel et al.* [1988] in assuming a volume flux through the Canadian Archipelago of 1.7 Sv. *Rudels* [1986] derives a volume flux of 0.7 Sv, while our model predicts 0.54 Sv. In any case, this is a significant amount of water, of the same order (or greater) as the flow in the same depth interval (the upper few hundred meters) of the East Greenland Current. Yet most models neglect the flow through the Canadian Archipelago, or assume it is small. For example, *Häkkinen* [1993] assumes a volume flux of 0.3 Sv, all through Nares Strait.

Further, the flow through the Canadian Archipelago is significant to the overall freshwater budget of the Arctic Ocean, since it drains the relatively fresh upper layer waters of the western Arctic. Our results indicate that the liquid freshwater flow through these channels is about 60% more than that in the East Greenland Current, and our simple climate change simulation suggests that CO_2-induced global warming would enhance the outflow of (liquid) freshwater through the Canadian Archipelago more than that through Fram Strait.

Acknowledgments. This work is supported as part of an EOS interdisciplinary investigation, Polar Exchange at the Sea surface (POLES), NASA grant NAGW-2407. S. M. also acknowledges the partial support of the Office of Naval Research, contract N00014-87-0160.

References

Aagaard, K., and E. C. Carmack, The role of sea ice and other fresh water in the Arctic circulation, *J. Geophys. Res., 94,* 14,485-14,498, 1989.

Aagaard, K., and L. K. Coachman, The East Greenland Current north of Denmark Strait: Part I, *J. Arctic Inst. North America, 21,* 181-199, 1968.

Aagaard, K., and P. Greisman, Toward new mass and heat budgets for the Arctic Ocean, *J. Geophys. Res., 80,* 3821-3827, 1975.

Aagaard, K., L. K. Coachman, and E. Carmack, On the halocline of the Arctic Ocean, *Deep Sea Res., 28,* 529-545, 1981.

Björk, G., A one-dimensional time-dependent model for the vertical stratification of the upper Arctic Ocean, *J. Phys. Oceanogr., 19,* 52-67, 1989.

Cavalieri, D. J., P. Gloersen, and W. J. Campbell, Determination of sea ice parameters with the Nimbus 7 SMMR, *J. Geophys. Res., 89,* 5355-5369, 1984.

Clarke, R. A., and J.-C. Gascard, The formation of Labrador Sea Water, I, Large-scale processes, *J. Phys. Oceanogr., 13,* 1764-1778, 1983.

Coachman, L. K., and K. Aagaard, Transports through Bering Strait: Annual and interannual variability, *J. Geophys. Res., 93,* 15,535-15,539, 1988.

Dickson, R. R., J. Meincke, S.-A. Malmberg, and A. J. Lee, The "Great Salinity Anomaly" in the Northern North Atlantic 1968-1982, *Prog. Oceanogr., 20,* 103-151, 1988.

Fissel, D.B., D.D. Lemon, H. Melling, and R.A. Lake, Non-tidal flows in the Northwest Passage, *Can. Tech. Rept. Hydrogr. Ocean Sci., 98,* Inst. of Ocean Sci., Sidney, B.C., Canada, 1988.

Foldvik, A., K. Aagaard, and T. Tørresen, On the velocity field of the East Greenland Current, *Deep Sea Res., 35,* 1335-1354, 1988.

Häkkinen, S., An arctic source of the Great Salinity Anomaly: A simulation of the Arctic ice-ocean system for 1955-1975, *J. Geophys. Res., 98,* 16,397-16,410, 1993.

Häkkinen, S., and G. L. Mellor, One hundred years of Arctic ice cover variations as simulated by a one-dimensional, ice-ocean model, *J. Geophys. Res., 95,* 15,959-15,969, 1990.

Hanzlick, D. J., and K. Aagaard, Fresh and Atlantic water in the Kara Sea, *J. Geophys. Res., 85,* 4937-4942, 1980.

Lascaratos, A., R.G. Williams, and E. Tragou, A mixed-layer study of the formation of Levantine Intermediate Water, *J. Geophys. Res., 98,* 14,739-14,749, 1993.

Lemke, P., and T. O. Manley, The seasonal variation of the mixed layer and the pycnocline under polar sea ice, *J. Geophys. Res., 89,* 6494-6504, 1984.

Lemke, P., W.B. Owens, and W.D. Hibler III, A coupled sea ice-mixed layer-pycnocline model for the Weddell Sea, *J. Geophys. Res., 95,* 9513-9525, 1990.

Levitus, S., Climatological atlas of the world ocean, *NOAA Prof. Pap. 13,* 173 pp., U.S. Gov. Print. Off., Washington, D. C., 1982.

MacDonald, R. W., E. C. Carmack, F. A. McLaughlin, K. Iseki, D. M. MacDonald, and M. C. O'Brien, Composition and modification of water masses in the Mackenzie shelf estuary, J. *Geophys. Res., 94,* 18,057-18,070, 1989.

Manabe, S., and R. J. Stouffer, Multiple-century response of a coupled ocean-atmosphere model to an increase of atmospheric carbon dioxide, *J. Climate, 7,* 5-23, 1994.

Manabe, S., M. J. Spelman, and R. J. Stouffer, Transient responses of a coupled ocean-atmosphere model to gradual changes of atmospheric CO_2, I, Annual mean response, *J. Climate, 4,* 785-818, 1991.

Manabe, S., M. J. Spelman, and R. J. Stouffer, Transient responses of a coupled ocean-atmosphere model to gradual changes of atmospheric CO2, II, Seasonal response, *J. Climate, 5,* 105-126, 1992.

Mellor, G. L., and L. Kantha, An ice-ocean coupled model, *J. Geophys. Res., 94,* 10,937-10,954, 1989.

Mellor, G. L., and T. Yamada, Development of a turbulence closure model for geophysical fluid problems. *Rev. Geophys., 20,* 851-875, 1982.

Mellor, G. L., M. G. McPhee, and M. Steele, Ice-Seawater turbulent boundary layer interaction with melting or freezing, *J. Phys. Oceanogr., 16,* 1829-1846, 1986.

Morison, J. H., and J. D. Smith, Seasonal variations in the upper Arctic Ocean as observed at T3, *Geophys. Res. Lett., 8,* 753-756, 1981.

Oort, A. H., L. A. Anderson, and J. P. Peixoto, Estimates of the energy cycle of the oceans, *J. Geophys. Res., 99,* 7665-7688, 1994.

Parkinson, C. L., Interannual variability of the spatial distribution of sea ice in the north polar region, *J. Geophys. Res., 96,* 4791-4801, 1991.

Pavlov, V. K., and S. L. Pfirman, Hydrographic structure and variability of the Kara Sea: Implications for pollutant distribution, *Deep Sea Res., 42,* 1369-1390, 1995.

Piacsek, S., R. Allard, and A. Warn-Varnas, Studies of the Arctic ice cover and upper ocean with a coupled ice-ocean model, *J. Geophys. Res., 96,* 4631-4650, 1991.

Riedlinger, S. H., and A. Warn-Varnas, Predictions and studies with a one-dimensional ice-ocean model, *J. Phys. Oceanogr., 20,* 1545-1562, 1990.

Rudels, B., The outflow of polar water through the Arctic Archipelago and the oceanographic conditions in Baffin Bay, *Polar Res., 4,* 161-180, 1986.

Rudels, B., On the mass balance of the Polar Ocean, with special emphasis on the Fram Strait, *Nor. Polarinstitutt Skr., 188,* 1-53, 1987.

Schlosser, P., G. Bönisch, M. Rhein, and R. Bayer, Reduction of deep-water formation in the Greenland Sea during the 1980's: Evidence from tracer data, *Science, 251,* 1054-1056, 1991.

Stigebrandt, A., A model for the thickness and salinity of the upper layer in the Arctic Ocean and the relationship between the ice thickness and some external parameters, *J. Phys. Oceanogr., 11,* 1407-1422, 1981.

Talley, L. D., and M. S. McCartney, Distribution and circulation of Labrador Sea Water, *J. Phys. Oceanogr., 12,* 1189-1205, 1982.

The Open University, *Ocean Circulation,* 238 pp., Pergamon, New York, 1989.

Thomas, D. R., and D. A. Rothrock, The Arctic Ocean ice balance: A Kalman smoother estimate, *J. Geophys. Res., 98,* 10,053-10,067, 1993.

Thomas, D., D. Rothrock, S. Martin, and M. Steele, Assimilating satellite concentration data into an Arctic sea ice mass balance model, 1979-1985, *J. Geophys. Res.,* this issue.

Thorndike, A. S., D. A. Rothrock, G. A. Maykut, and R. Colony, The thickness distribution of sea ice, *J. Geophys. Res., 80,* 4501-4513, 1975.

Untersteiner, N., and A. S. Thorndike, Arctic data buoy program, *Polar Record, 21,* 127-135, 1982.

Vowinckel, E., and S. Orvig, The climate of the North Polar Basin, in *World Survey of Climatology,* vol. 14, *Climates of the Polar Regions,* edited by S. Orvig, pp. 129-252, Elsevier, New York, 1970.

Wallace, D. W. R, R. M. Moore, and E. P. Jones, Ventilation of the Arctic Ocean cold halocline: Rates of diapycnal and isopycnal transport, oxygen utilization and primary production inferred using chlorofluoromethane distributions, *Deep Sea Res., 34,* 1957-1979, 1987.

Wijffels, S. E., R. W. Schmitt, H. L. Bryden, and A. Stigebrandt, Transport of freshwater by the oceans, *J. Phys. Oceanogr., 22,* 155-162, 1992.

S. Martin, Department of Oceanography, College of Ocean and Fishery Sciences, University of Washington, Seattle, WA 98105.

D. Rothrock, M. Steele, and D. Thomas, Polar Science Center, Applied Physics Laboratory, College of Ocean and Fishery Sciences, University of Washington, Seattle, WA 98105

(Received May 3, 1995; revised May 1, 1996; accepted May 6, 1996.)